Rose Bengal analogs and vesicular glutamate transporters (VGLUTs)

Nicolas Pietrancosta [a], Albane Kessler [a,†], Franck-Cyril Favre-Besse [a], Nicolas Triballeau [a,‡], Thomas Quentin [b,c,d], Bruno Giros [b,c,d,e], Salah El Mestikawy [b,c,d,e], Francine C. Acher [a,*]

[a] Laboratoire de Chimie et Biochimie Pharmacologiques et Toxicologiques, UMR8601 CNRS, Université Paris Descartes, 45 rue des Saints-Pères, 75270 Paris 06, France
[b] Centre National de la Recherche Scientifique (CNRS) UMR 7224, Université Paris 6, Pathophysiology of Central Nervous System Disorders, 9 quai Saint Bernard, 75005 Paris, France
[c] Institut National de la Santé et de la Recherche Médicale (INSERM), U952, Université Paris 6, Pathophysiology of Central Nervous System Disorders, 9 quai Saint Bernard, 75005 Paris, France
[d] Université Pierre et Marie Curie, UPMC, Université Paris 6, Pathophysiology of Central Nervous System Disorders, 9 quai Saint Bernard, 75005 Paris, France
[e] Douglas Hospital Research Center, Department of Psychiatry, McGill University, 6875 Boulevard Lasalle Verdun, QC, Canada

ARTICLE INFO

ABSTRACT

Vesicular glutamate transporters (VGLUTs) allow the loading of presynaptic glutamate vesicles and thus play a critical role in glutamatergic synaptic transmission. Rose Bengal (RB) is the most potent known VGLUT inhibitor (K_i 25 nM); therefore we designed, synthesized and tested in brain preparations, a series of analogs based on this scaffold. We showed that among the two tautomers of RB, the carboxylic and not the lactonic form is active against VGLUTs and generated a pharmacophore model to determine the minimal structure requirements. We also tested RB specificity in other neurotransmitter uptake systems. RB proved to potently inhibit VMAT (K_i 64 nM) but weakly VACHT (K_i >9.7 μM) and may be a useful tool in glutamate/acetylcholine co-transmission studies.

1. Introduction

The neurotransmitter cycle is an essential step in synaptic transmission. Neurotransmitters released from synaptic vesicles by exocytosis bind to various receptors to produce their biological response. Extraneuronal neurotransmitters are then removed from the synaptic cleft by uptake sites located in the plasma membrane.[1,2] Once in the cytoplasma, neurotransmitters accumulates into synaptic vesicles for additional cycles of release.[3–5] The combined actions of the plasma membrane and vesicular transporters maintain the proper concentrations of extracellular neurotransmitter before, during and after neurotransmission.[6,7] Glutamate, the major excitatory neurotransmitter in the mammalian central nervous system (CNS), is involved in most, if not all, physiological functions as well as neuropathologies of the CNS.[8–17]

In this study, we focus our attention on one step of the glutamate cycle: the vesicular accumulation uploading by vesicular glutamate transporters (VGLUTs). Three different isoforms of VGLUTs have been identified (VGLUT1–3) sharing a high degree of sequence homology (more than 75%) but with almost complementary distributions of VGLUT1 and VGLUT2, and a more restricted expression of VGLUT3 in a small set of neurons releasing other neurotransmitters.[1,18–21] Recently, a relevant correlation between Alzheimer associated dementia and VGLUT1 disappearance has been described.[22] This study contributes to investigations on VGLUT markers and/or modulators as potential early diagnostic tools in AD.[23,24]

Despite their key role in excitatory transmission, very few chemical compounds efficiently target this family of glutamate
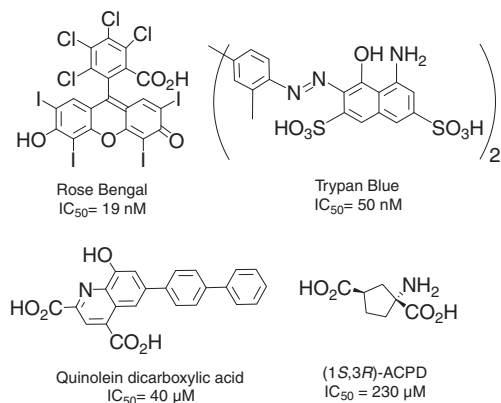
Figure 1. Different families of known VGLUTs ligands.

transporters.[1] The need of pharmacological tools is now crucial to understand better the functional implication of VGLUT1–3 in normal and pathological conditions and to use them as biomarkers of human 'synaptopathologies' for diagnosis or therapeutic purposes. Presently, three types of VGLUT inhibitors have been identified[1] (Fig. 1): dyes[5,25–33] with K_i in the 20 nM to 10 μM range (e.g., Rose Bengal and Trypan Blue), substituted quinolines[29,34,35] with K_i in the 40–300 μM range and glutamate analogs with IC$_{50}$ >230 μM (e.g., (1S,3R)-ACPD). Dyes display higher affinities, probably because of their hydrophobic aromatic part, but a lower selectivity than quinolines.[2] Among them, Rose Bengal (RB) is the only non-competitive inhibitor and it exhibits the highest affinity of all (K_i 19 nM);[36] the third type includes the glutamate-like inhibitors known to interact with glutamate receptors but these compounds show very poor activity on vesicular glutamate uptake.[1] We may explain these results by the low affinity of VGLUTs against glutamate, its physiological substrate (K_m(Glu) >1 mM).

The original aim of this study was the design of new VGLUT binding compounds with improved affinity and selectivity. Since RB was the most potent known inhibitor, we chose to synthesize various derivatives **1**–**8** and to evaluate them as glutamate uptake inhibitors in a 96-well plate assay. Their activities were merged with those of commercially available dyes that had been previously tested (**BU1** to **BU15** in Table 1)[33] to establish a structure–activity relationship and to generate a pharmacophore model. This model allowed to define the chemical and spatial features of RB that are required for potent vesicular glutamate transport inhibition. To assess its selectivity, we also examined the efficacy of RB (**2b**) on the vesicular monoamine transporter (VMAT) and vesicular acetylcholine transporter (VACHT). Since RB is a non-competitive inhibitors, we discuss its possible binding to other proteins involved in glutamate transport.

2. Results and discussion

2.1. Chemistry

All synthesis of fluorescein analogs that were described follow the same strategy[37–39] that we also adopted. Synthesis of compounds **2** was performed in two steps: coupling of phthalic anhydride with resorcinol to afford fluorescein derivatives[40] **1** and subsequent introduction of iodine onto the xanthene moiety (Scheme 1).[41] For the poly-condensation, two methods have been described in the literature with Brønsted or Lewis acids. After comparing these two methods (methane sulfonic acid[42] or ZnCl$_2$[43]), we selected the zinc chloride catalysis protocols due to higher yields and easier workup. In this protocol, the two reagents are crushed together, pooled with zinc chloride and the neat mixture heated

at 180 °C before refluxing in methanol. The expected product is obtained in a good crude yield after extraction and engaged directly in the next step without further purifications. The yields for these condensations varied from 21% to 59%.
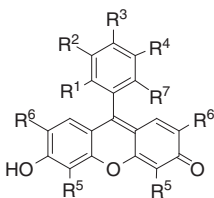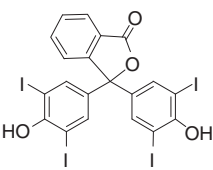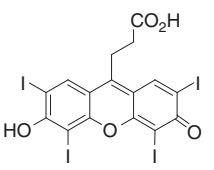
The mechanism of the condensation step involves a multiple and successive Friedel and Craft acylation (Scheme SI-1). This sequential mechanism allows the synthesis of asymmetrical[43] and symmetrical compounds such as **6** and **7** in which the first attack is performed by the 1,3-dihydroxynaphthalene followed by resorcinol attack for **6** (Fig. 2).

Additionally, this mechanism (Scheme SI-1) determines the positions of the R$^{1-4}$ substituents in compounds **1** and subsequently in **2** in Scheme 1. Starting with mono-substituted phthalic anhydrides, a single or a mixture of two regioisomers could be formed with substituents at R^{1,4} (**1h**, **1j**) or R^{2,3} (**1i**, **1k**, **1l**) positions. The first nucleophilic attack of resorcinol on the phthalate derivative occurred at the most electrophilic carbonyl (Scheme SI-1), but in the case of compounds **1h**, **1i**, **1k**, **1l** the two phthalic carbonyls appeared to display an equivalent electrophilicity and a mixture of two isomers for each compound was obtained[40] (Scheme SI-2A). In order to confirm this hypothesis, we performed the ^{13}C NMR spectra of starting materials (i.e., phthalate derivatives) assuming that the chemical shifts of the carbonyl carbons could be correlated to their reactivity against nucleophilic attack. We observed that when the difference of carbonyl ^{13}C chemical shift of starting phthalate anhydride was less than 2 ppm, two regioisomers were obtained (i.e., **1h**, **1i**, **1k**, **1l**) but in the case of compound **1j** only one isomer was identified by ^{1}H NMR (Table SI-2). This is probably due to the delocalization of oxygen electrons of the hydroxyl group through the beta carbonyl resulting in its deactivation (Scheme SI-1B). The different isomers were not separated and each mixture was evaluated for its uptake inhibitory activity. As none of the tested compounds appeared to have significant activity (see below), the separation was definitively not carried out although some recrystallization protocols have been described in which protection deprotection steps were required.[40,44–46]

The last step of the synthesis consists in the insertion of iodine in the xanthene moiety. Among the different classical methodologies, we have selected one of the smoothest (I$_2$/HIO$_3$ in EtOH).[41] This method leads to the desired compounds **2** without detection of any partial iodination (Scheme 1). Moreover, this strategy is suitable for the final purification processes. Indeed, one of the major difficulties of this synthesis consists in the purification and the characterization of the compounds that revealed not to be trivial: these molecules are highly aromatic and planar, they are subjected to π-stacking which also explains their low solubility in common organic solvents.[47] Introduction of iodine or bromine atoms confers to them a high degree of anisotropy. In most cases, the remaining protons of the molecules do not relax properly and the ^{1}H NMR spectra were very sluggish with broad signals. Similarly, ^{13}C NMR spectra could not be recorded. Variation of temperature could not improve the quality of the spectra, neither did dilution of the samples. Moreover, only one ^{1}H NMR peak is expected with the more soluble lactonic tautomer.[48–50] Compounds were thus characterized by mass spectrometry and their purity assessed by HPLC. A HPLC method was set up using a C18 column and a methanol/water gradient as eluent (see below). Mass spectroscopy (negative electrospray ESI$^-$) of the crude precipitated compound showed in most cases a single peak corresponding to [M−H]$^-$. In few cases, we have observed the corresponding positive peak in ESI$^+$ mode.

A tautomeric equilibrium between a carboxylic and lactonic form of fluorescein derivatives is known to take place (Scheme 2). Christophersen et al. have demonstrated the structure of red and orange fluorescein, that is, tautomeric forms, by a combination of solution and solid state ^{13}C NMR methods.[51] Importantly this equilibrium is pH dependent. Fluorescein derivatives exist in four

Table 1
Activities of newly synthesized (**1–8**) compounds and of those previously tested and numbered **BU1–15**[33]

1-3,6,7,8 and BU1-BU3, BU5-BU12, BU14, BU15   **BU13**   **BU4**

Entry	R1	R2	R3	R4	R5	R6	R7	IC$_{50}$ nM (n)
2b	Cl	Cl	Cl	Cl	I	I	CO$_2$H	25 ± 3.2 (9)
2c	Cl	H	H	Cl	I	I	CO$_2$H	27 ± 4.1 (3)
2a	H	H	H	H	I	I	CO$_2$H	36 ± 6.5 (6)
2d	H	Cl	Cl	H	I	I	CO$_2$H	41 ± 8.4 (3)
BU1	Cl	Cl	Cl	Cl	I	I	CO$_2$Me	44
BU6	Cl	Cl	Cl	Cl	Br	Br	CO$_2$H	51
BU2	Cl	Cl	Cl	Cl	I	I	CO$_2$Bn	65
BU9	H	H	H	H	Br	Br	CO$_2$Et	65
BU14	Cl	Cl	Cl	Cl	I	I	H	68
2f	Br	Br	Br	Br	I	I	CO$_2$H	74 ± 11.7 (3)
2e	F	F	F	F	I	I	CO$_2$H	102 ± 5.4 (3)
BU10	H	H	H	H	Br	Br	CO$_2$Me	117
4[a]	Cl	Cl	Cl	Cl	I	I	CO$_2$H	123 ± 17.4 (4)
3	Cl	Cl	Cl	Cl	I	I	CO$_2$Et	192 ± 5 (4)
8	H	H	H	H	Br	NO$_2$	CO$_2$Et	238 ± 9 (2)
2i[b]	H	CO$_2$H	H	H	I	I	CO$_2$H	288 ± 71 (3)
	H	H	CO$_2$H	H	I	I	CO$_2$H	
BU7	H	H	H	H	Br	Br	CO$_2$H	406
2g	H	H	H	H	CH$_3$	I	CO$_2$H	531 ± 175 (3)
BU3	H	NCS–	H	H	I	I	CO$_2$H	689
2k[b]	H	CH$_3$	H	H	I	I	CO$_2$H	987 ± 137 (3)
	H	H	CH$_3$	H	I	I	CO$_2$H	
BU5	H	H	H	H	I	H	CO$_2$H	1060
BU4	–	–	–	–	I	I	CO$_2$H	2200
BU8[c]	H	H	H	H	Br	NO$_2$	CO$_2$H	2445
BU13[c]	H	H	H	H	I	I	CO$_2$H	3850
2l[b]	H	tBu	H	H	I	I	CO$_2$H	5925 ± 3685 (2)
	H	H	tBu	H	I	I	CO$_2$H	
2h[b]	NO$_2$	H	H	H	I	I	CO$_2$H	6690 ± 2048 (2)
	H	H	H	NO$_2$	I	I	CO$_2$H	
2j	H	H	H	OH	I	I	CO$_2$H	7800 ± 648 (2)
5[c,d]	Cl	Cl	Cl	Cl	I	I	CO$_2$H	8824 ± 1119 (2)
BU11	Cl	Cl	Cl	Cl	H	H	CO$_2$H	15,000
BU15	H	H	H	H	OH	H	SO$_3$H	>32,000
BU12	H	H	H	H	H	Cl	CO$_2$H	>64,000
1a	H	H	H	H	H	H	CO$_2$H	Inactive (3)
6	Cl	Cl	Cl	Cl	H	Mono-naphthyl	CO$_2$H	Inactive (3)
7	Cl	Cl	Cl	Cl	H	Di-naphthyl	CO$_2$H	Inactive (3)

Data from this study and literature may be compared on the same scale since Erythrosin B (**2a**) and RB (**2b**) display similar activities in both studies.
  [a] RB monoether.
  [b] Mixture of the two diastereoisomers.
  [c] Lactone form.
  [d] RB diether. Each concentration has been measured in triplicate and data are the mean ± SEM of n separate experiments.

protonated states (neutral form, monoanion A or B, dianion, Scheme 3) because of two ionizable groups. In the fluorescein **1** series, substituents present in the xanthene moiety (R^5 and R^6, Scheme 3) highly influence the pK_a of the phenolic oxygen, while when in the phenyl ring (R^1–R^4, Scheme 3) they only modulate the pK_a of the carboxylic acid. Several authors have shown that the lactone form is only found with the neutral form and not with mono- or dianion forms.[39,48,52] Consequently at physiological pH most tested derivatives are only found in the carboxylic tautomeric form because of deprotonation of their carboxylic and phenolic groups. However some exceptions were described. In fact, fluorescein analogs bearing mesomer acceptor substituents (e.g., NO$_2$) in *ortho* positions to the phenol groups (R^5 and R^6 in Scheme 3, **BU8** in Table 1) as well as phenolphthalein derivatives (**BU13** in Table 1) are only found as lactones at neutral pH.[53–56]

Thus a key point was to identify which form between carboxylic acid and lactone of all tested analogs, occurs in biological conditions (pH 7.2). Indeed the two tautomers exhibit different 3D conformations as well as diverse ability to contract some protein interactions and thus reveal different pharmacological effects. As RB and RBL (Rose Bengal lactone) are commercially available, and their spectral properties described, UV absorption of these two samples in a pH 7.2 phosphate buffer were measured. The two spectra are totally identical and the same as described for RB open form (different from RBL), showing that in these conditions, the RBL opens up (Scheme 3). In order to further characterize which forms of compounds **2** are present in solution, they were analyzed by HPLC on a C18 column eluted with a methanol/water gradient. Open compounds showed retention times around 15 min whereas cyclized forms were less retained with a retention time ranging from 5 to 8 min. RB and RBL dissolved in a
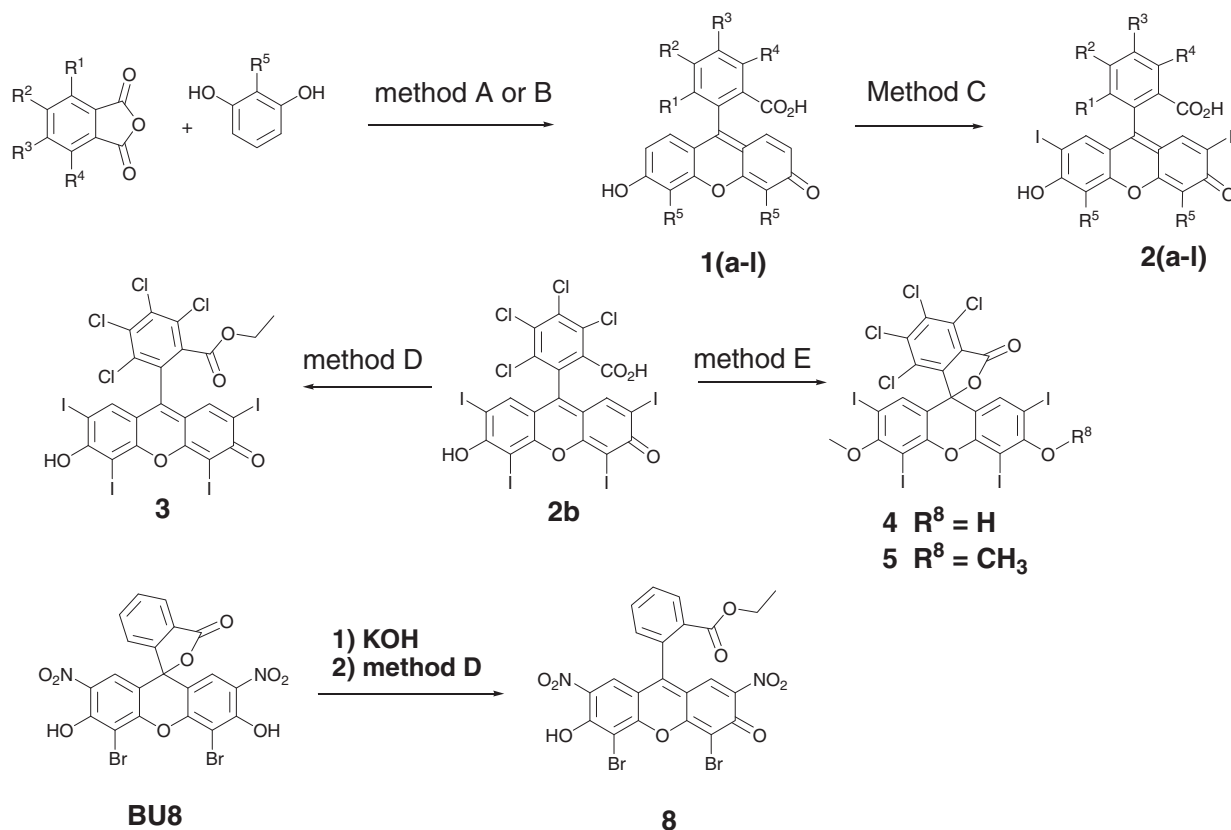
Scheme 1. Formation of fluorescein derivatives by condensation of phthalic anhydride and resorcinol and subsequent iodination. 1: R^5 = H, 2: R^5 = I, a: R^1 = R^2 = R^3 = R^4 = H; b: R^1 = R^2 = R^3 = R^4 = Cl; c: R^1 = R^4 = Cl, R^2 = R^3 = H; d: R^1 = R^4 = H, R^2 = R^3 = Cl; e: R^1 = R^2 = R^3 = R^4 = F; f: R^1 = R^2 = R^3 = R^4 = Br; h: R^1 = NO$_2$, R^2 = R^3 = R^4 = H and R^1 = R^2 = R^3 = H, R^4 = NO$_2$; i: R^1 = R^3 = R^4 = H, R^2 = CO$_2$H and R^1 = R^2 = R^4 = H, R^3 = CO$_2$H; j: R^1 = R^2 = R^3 = H, R^4 = OH; k: R^1 = R^3 = R^4 = H, R^2 = CH$_3$ and R^1 = R^2 = R^4 = H, R^3 = CH$_3$; l: R^1 = R^3 = R^4 = H, R^2 = t-Bu and R^1 = R^2 = R^4 = H, R^3 = t-Bu; g: R^1 = R^2 = R^3 = R^4 = H R^5 = CH$_3$. Reagents and conditions: (a) method A: CH$_3$SO$_3$H, 80 °C; method B: ZnCl$_2$, 180 °C, neat; method C: HIO$_3$/I$_2$/EtOH; method D: Et-Br, DBU, THF, 65 °C; method E: CH$_3$I/DMF, rt.
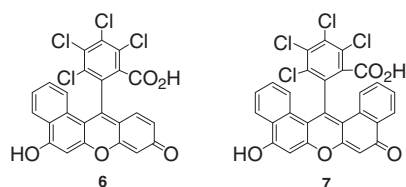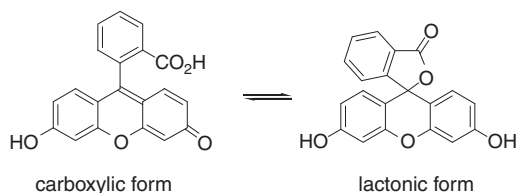

Figure 2. Structure of compounds **6** and **7**.


carboxylic form   lactonic form

Scheme 2. Tautomeric equilibrium of fluorescein.

pH 7.2 phosphate buffer eluted both as RB at 15.80 min (Fig. SI-1). Carboxylic form of fluorescein and iodinated analogs in basic conditions was also confirmed by HPLC. Finally to identify which of the tautomeric forms binds to the transporters VGLUTs, we synthesized various analogs locked in the carboxylic or lactonic form (**3–5**, **8** scheme 1). The esterified compounds **3** and **8** were obtained by reaction of ethyl bromide with RB in the presence of DBU in THF. Different methodologies have been described for the etherification of

phenol derivative as Mitsunobu reaction or methyl iodide alkylation. Compound **4** was obtained by direct alkylation of RB lactone by methyl iodide in THF. To block Rose Bengal in its cyclized form, we performed the O-methylation of both phenolic oxygens with 2 equiv of methyl iodide affording diether **5**. Unlike **3** and **5**, **4** may still undergo the tautomeric equilibrium (Scheme 3) which is shifted to the carboxylic form at neutral pH.[57,58]

2.2. VGLUTs Pharmacology

In order to rationalize the synthesis of the new compounds, we thought to use the structure–activity study (SAR) performed by Bole and Ueda (entries **BU1** to **BU15** in Table 1).[33] As mentioned previously, all Rose Bengal derivatives may exist in either carboxylic or lactonic forms (Scheme 2). A large number of physicochemical studies (pH- and solvent-dependent) on fluorescein derivatives, focused on the equilibrium between the different tautomers, have been published.[52,59–61] Yet, Bole and Ueda[33] left out this point and considered that carboxylic acid and lactone of RB analogs remained as two different chemical entities in aqueous solution. Consequently, we thought that the RB SAR study of VGLUT inhibition needed to be revisited. The new and former pharmacological data were analyzed and allowed to determine the structural requirements for VGLUT inhibition by RB analogs. The RB analogs were first tested with the commonly used [³H]-Glu vesicular uptake assay in the presence (or absence) of inhibitors at various concentrations, as previously described.[62] This type of assay was technically incompatible with structure–activity studies because of the limited number of compounds that could be tested simultaneously. Hence, a 96-well plate
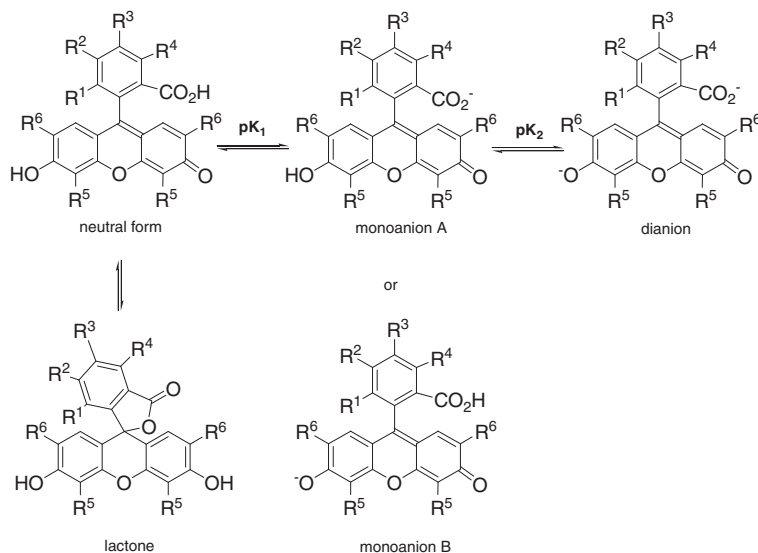
Scheme 3. Protonation state of fluorescein derivative tautomers at various pH. Monoanion A or B are present according to R^5 and R^6 substituents that influence the pK_a of the phenol. For R^1–R^6 see Scheme 1 and Chart SI.

assay was set up and validated with the following controls. Activity measures in this up-scaled assay and classical assay proved to be comparable as demonstrated with RB (**2b**) and Erythrosin B (**2a**) (Table 1). IC_{50} values of 25 nM and 36 nM for **2b** and **2a**, respectively, were obtained with the 96-well plate assay that compare to 22 nM and 35 nM obtained by Bole and Ueda.[33] Moreover, the 96-well plate assay increased the robustness of data and allowed higher precision in the IC_{50} determination. It also highlighted the solubility troubles encountered with RB derivatives even at low micromolar concentrations while this problem was not easily detected in the traditional assay (reduced filter diameter in the 96-well plate assay). As mentioned previously, the Rose Bengal analogs are sparingly soluble in various organic solvents such as dimethylsulfoxide (DMSO) traditionally used for compound solubilization. In order to be sure about the tested concentration, our analogs were dissolved in the transport biological buffer. The compounds were then filtered and the concentration confirmed by HPLC analysis as described by Bole and Ueda.[33] The activities of all new compounds are reported in Table 1 together with literature data of compounds **BU1–BU15**.[33] These two sets of IC_{50}'s can be directly compared since two compounds **2b** (RB) and **2a** (Erythrosin B) which were used to calibrate the assay displayed similar values in both studies (see above). Altogether the improvement of the uptake assay resulted in rapid and reliable evaluation of our new compounds.

2.3. Structure–activity relationship

VGLUT inhibitors listed in Table 1 (structures displayed in Chart SI) were ranked in order of potency. Among the 17 new compounds none was more efficient than RB (**2b**). The monoether derivative **4** that may still undergo the tautomeric equilibrium and is mostly found as carboxylic acid at neutral pH, was used as a probe of phenolic methylation when its activity was compared to that of **5**. On the other hand, the role of the RB carboxylic group was defined by comparison of the inhibitory effect of descarboxy RB (**BU14**) with that of RB (**2b**). While **3**, **4**, **8**, **BU1**, **BU2**, **BU9**, **BU10** and **BU14** still reasonably inhibited glutamate transport, analogs **5** and **BU8** required at least one or two log higher concentration. Although not as hydrophobic, the R^6 nitro group of **BU8** is neutral, electron attracting and sterically similar to the iodo substituent of **2a** and **2g** (Fig. SI-2). Moreover, ester **8** of opened lactone **BU8**, was as

potent as RB ester **3** and one log more potent than **BU8**. We can thus conclude that the bioactive form of Rose Bengal is the carboxylic form which is indeed the predominant form in aqueous solution buffered at pH 7.2 for biological assays. The loss of planar structure and loss of conjugation of the xanthyl moiety with C'_9 sp^3 hybridized may be the cause of the reduced activity of RB lactones and **BU13**. Such an observation would be in line with a flat hydrophobic binding site.

As previously reported,[33] positions 2′, 4′, 5′, 7′ (R^5 and R^6 Table 1) of the fluorescein xanthyl part require iodine or bromine substitutions. Comparison of IC_{50}'s of **2b** and **BU6** with **BU11** revealed a decrease of over two orders of magnitude when I or Br were replaced by H. This critical role is confirmed by the reduced effect of **1a** and **BU5** compared to **2a**. Any other substitutions with smaller or larger groups (Fig. SI-2) decreased the inhibitory potency: compound **2g** in which two iodines were replaced by a methyl group was 20 times less active than the tetraiodo analog **2a** (Erythrosin B) and the bulky compounds **6** and **7** were totally inactive at a 2.5 µM concentration.

Regarding the phenyl part of fluorescein analogs, it may not be replaced by a linear chain since **BU4** is poorly active but the presence of four chlorine atoms at positions 4–7 is not mandatory since **2a** (4xH), **2b** (4xCl) and **2c** (2xCl) are equipotent and **2f** (4xBr) and **2e** (4xF) only slightly weaker. Because of this relative lenience, we designed a series of **2a** analogs varying the phenyl substituents. However while halogens were well accommodated decreasing from chlorine (**2b** and **2c**) to bromine (**2f**) and fluorine (**2e**) and even hydrogen (**2a**), other substitutions were deleterious. Introducing a polar substitution at position 4, 7 (R^1, R^4) such as NO_2 in **2h**, OH in **2j** or at position 5, 6 (R^2, R^3) such as CO_2H in **2i** resulted in a drop of activity. Hydrophobic groups at position 4, 7 (R^1, R^4) induced an even more dramatic loss with a methyl group in **2k** and a *tert*-butyl in **2l**. The carboxylic group at position 3 of the phenyl ring (R^7 in Table 1) is unnecessary for binding but useful for aqueous solubility. Actually this group may be esterified to methyl, ethyl or benzyl ester or even removed (**BU14**) without major loss of potency. This observation suggests the design of a new ester library that could be obtained by easy esterification of **2b** with diverse alcohols. Previous studies have taken advantage of that carboxylic function in **2b** to link fluorescent RB to various active principles (e.g., peptides, alkyl chains).[63,64] Such a substitution

may thus enable to reach a specific pocket that would increase the specificity of the inhibitor.

Altogether halogen substitutions at the xanthyl and phenyl ring of RB (**2b**) are the most critical. A specific interaction between halogens and oxygen atoms from proteins and in particular from backbone carbonyls has been recently reported.[65] This halogen bonding was demonstrated to stabilize several protein kinase–inhibitor complexes. Such interactions may also be involved in RB–VGLUT complex and would explain the unique properties of halogen substituents in RB. Alternatively, the halogen atoms may be binding in a hydrophobic cavity that would be best fitted with iodine.

2.4. VGLUT pharmacophore model generation

Overall the SAR data allowed us to generate a pharmacophore model of RB VGLUT inhibitors. The modeling part of this study was performed with version 2.5 of the Discovery Studio suite available from Accelrys Inc. (San Diego CA, USA).

Each molecule was drawn in its predominant tautomer and its major protonated state at the pH used for the biological tests (pH 7.2), as determined above. To ensure proper conformational coverage, each isomer of compounds available in mixtures (**2h**, **2i**, **2k**, **2l**) was drawn separately yielding a total of 37 molecules. Conformational expansion was performed with Catalyst-CatConf[66,67] using the BEST mode and an energy window of 10 kcal/mol above the global minimum. It is worth to note that the opened structures of fluorescein derivatives can be drawn with two major tautomeric forms with one phenolic and one quinonic form on each side of the central pyran ring of the xanthene system yielding a totally symmetric structure. Despite this symmetry DS Pharmacophore (i.e., the embedded Catalyst engine) is unable to perceive the two side rings as equivalent when feature mapping is performed. In order to address this point, the default Ring_Aromatic feature was edited to allow equivalent perception of the phenolic and quinonic parts of the molecular graph. Secondly, the default HB_Acceptor feature was modified to forbid the mapping of some weak H-bond acceptors present in the dataset (ether oxides, divalent oxygen atoms of esters, nitro groups and phenolic oxygens hindered by dual substitution in *ortho* and *ortho′*). Finally, a novel feature was designed to account for the presence of electron-withdrawing groups at certain positions of many compounds of the dataset and which could play a significant role in explaining the SAR. This new feature matches with nitro, cyano, trifluoromethyl, fluoryl, chloryl, ketonic and acidic moieties.

Pharmacophore model perception was performed using Catalyst-HypoGen executable from the '3D QSAR Pharmacophore Perception' protocol available from Discovery Studio 2.5 which invokes Catalyst-HypoGen via a PipelinePilot server.[68]

The training set consists in a selection of 18 compounds that regularly span the activity range: **2c**, **2a**, **BU1**, **BU6**, **2e**, **BU10**, **4**, **BU7**, **2g**, **BU5**, **BU4**, **BU13**, **2j**, **BU11**, **BU15**, **BU12**, **1a** and **7**. Their respective activities were kept as measured and their uncertainties set to 3. HypoGen was then left free to select the most relevant features among HYDROPHOBIC, Ring_Aromatic, HB_Acceptor and electon-withdrawing group with a minimum interfeature distance set at 2 Å. Several runs were performed with weights and/or tolerances kept fixed or authorized to vary.

The next step consists in the model validation. Indeed, Catalyst-HypoGen is a pharmacophore model perception method that determines minimum sets of features capable to explain the differences in activities among a collection of compounds spanning typically 3 to 4 logs of activities.[68] Its heuristic is divided in three phases. First of all, a constructive phase builds the pharmacophore space from the two most potent compounds keeping the configurations that matches with the rest of the most active molecules.

A subtractive phase then discards the solutions that can be mapped by a majority of inactive compounds. Finally, an optimization phase relaxes the remaining models via a simulated annealing algorithm. During this last phase, features are to some extent modified (their type, position, and, optionally, their weights and tolerances) in order to find a fit that better correlates with the measured activities. In the present case the generated models are combinations of four types of features: hydrophobic, ring aromatic, H-bond acceptor and electron-withdrawing group exhibiting either fixed or variable weights and tolerances. The retained models are those that exhibit a limited computational cost to describe the SAR, but they should also predict the activities within the correct log range (i.e., root mean square 'RMS' below 1 log of activity) and show acceptable discriminatory power between most active and least active compounds (area under the ROC curve >0.8). The best theoretical model ('fixed cost') and the worst ('null cost') serve as references to determine the quality of the generated models (Table 2).

Here, the use of variable weights allowed to slightly improve the RMS of the best model from 1.02 to 0.98 log of activity while retaining the same features and tri-dimensional dispositions as of the best model obtained with fixed weights (data not shown). This means that the additional complexity (i.e., cost) introduced while allowing weight variation is mostly due to the use of variable weights. It was therefore decided to retain this model because weights introduce an extra facet in the SAR analysis providing insight into the contribution of each feature to the activity. This model (Fig. 3) consists of four features: two ring aromatic A1 and A2 (one for each side ring of the xanthene system with weights of 2.9 and 2.25) and two hydrophobic features H1 at R^5 position of the xanthene moiety (weight: 2.25) and H2 located on the orthogonal phenyl substituent (weight 1.58). The presence of the two ring aromatic features A1 and A2 together with their total weight of 5.15 underscores the importance of the planarity of the tricyclic xanthene system. Indeed open structures such as **BU13** exhibit a strong angle between its lateral rings. Other structures like **7** adopt a twisted helicene-like conformation thus limiting the fit of such compounds and explaining their inactivity on VGLUTs.

The second most important feature in terms of weight is H1. If one considers the planar compounds which can fit the two ring aromatics, H1 correctly discriminates between the most active compounds exhibiting iodine, bromine or methyl at the R^5 position from the compounds bearing a hydrogen or a hydrophilic substituent at this very position: roughly, compounds that correctly map A1 and A2 but not H1 have an IC_{50} above 2.5 μM. H2 finally explains the limited activity of compounds such as **BU4** which does not have the orthogonal phenyl moiety or lactonic compounds such as **BU13** which are endowed with such a group but cannot project it to the correct location due to the tetrahedric geometry of the central carbon atom. Its lowered weight however does not penalize enough some compounds such as **2i** and **2j** which, despite hydrophilic substituents in R^4, are still overestimated by the model. This is a known limitation of pharmacophore perception with Catalyst-HypoGen which focuses only on the presence (or absence) of features *contributing* to the activity but does not account for the presence of features *penalizing* the activity (here hydrophilic substituents at the R^4 position).

It is worth to note that neither HB_Acceptor nor electron-withdrawing group features were retained in this model. In particular, Catalyst-HypoGen could have used such features to depict the SAR of the various orthogonal phenyl substituents. A comparison between **2b** (RB), **BU1**, **BU2** and **BU14** which all have IC_{50} of the same order of magnitude and only differ by their various HB_Acceptor moiety allows to understand the irrelevance of this feature. It is quite remarkable in fact that there is such little activity differences between a strong negatively charged function (**2b**, RB), a neutral weaker acceptor (**BU1**), a bulky substituent (**BU2**) or a simple

Table 2
Results obtained with the best models (model with lowest cost of 10 retained hypotheses after each run) obtained during the different runs performed with fixed and/or variable weights and tolerances

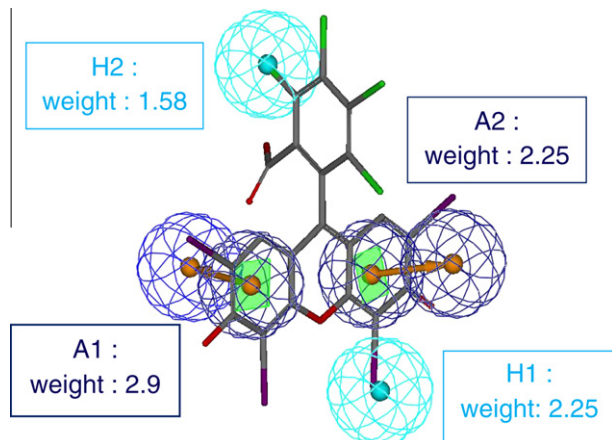| Parameters/model	Cost			RMS			ROC (AUC)		
	Fixed	Best	Null	Fixed	Best	Null	Fixed	Best	Null
Default (fixes weights and tolerances)	75	85			1.02			0.94	
Variable tolerances	88	99	119	0	1.02	2.56	1	0.95	0.5
Variable weights	87	96			0.98			0.94	
Var. tolerances and weights	100	109			0.99			0.93	

Figure 3. Selected VGLUTs pharmacophore model with Rose Bengal displayed (atom colors: carbon gray, oxygen red, chlorine green, iodine purple). Specific features are represented as colored spheres (dark blue: A1 and A2 ring aromatic, cyan: H1 and H2 hydrophobic features).

hydrogen (**BU14**). To explain these observations, we propose that the carboxyl moiety is pointing toward the solvent. Although we can not comment the mapping of **2h**, **2i**, **2k** and **2l** because the activity of each isomer could not be resolved from the obtained mixtures, the remaining test set compounds (**RB**, **2d**, **2f**, **4**, **BU2**, **BU3**, **BU8**, **BU9**, **BU14**, **6**, **8**) were all predicted in their actual log of activity at the exception of **5** (overestimated). Clearly the lactonic form of compounds such as **BU8**, **BU13** and **5** seem detrimental to the activity but, as stated before, unfavorable features are not properly considered during HypoGen runs.

2.5. VMAT2 and VACHT Pharmacology

In parallel to the structure/activity studies, and in order to evaluate more carefully the potentiality of this scaffold as VGLUT markers/modulators, we decided to examine the specificity of Rose Bengal (**2b**) with regards to other families of vesicular neurotransmitter transporters.[69] We assessed the efficacy of RB (**2b**) to inhibit the vesicular H^+-dependent accumulation of glutamate, monoamine (5-HT)[69,70] and acetylcholine mediated by the respective transporters (VGLUTs, VMAT2 and VACHT) (Fig. 4).

As previously reported, Rose Bengal inhibited glutamate vesicular uptake (IC_{50} 25 ± 1.1 nM, with a Hill number of 1.06 ± 0.08, Fig. 4). However, unexpectedly Rose Bengal was also able to inhibit H^+-dependent [^3H]-5-HT accumulation with an IC_{50} 64 ± 1 nM and Hill number of 1.7 ± 0.12. On the other hand, the efficiency of RB (**2b**) in acetylcholine uptake experiments was markedly low with no significant effect between 0.01 and 1 μM (extrapolated $IC_{50} \approx 9.7 ± 2.3$ μM). Such results are surprising since VMAT and VACHT belong to the same SLC18 family and VGLUTs to a related but distinct SLC17 family.[71] Yet, taking advantage of its preferred
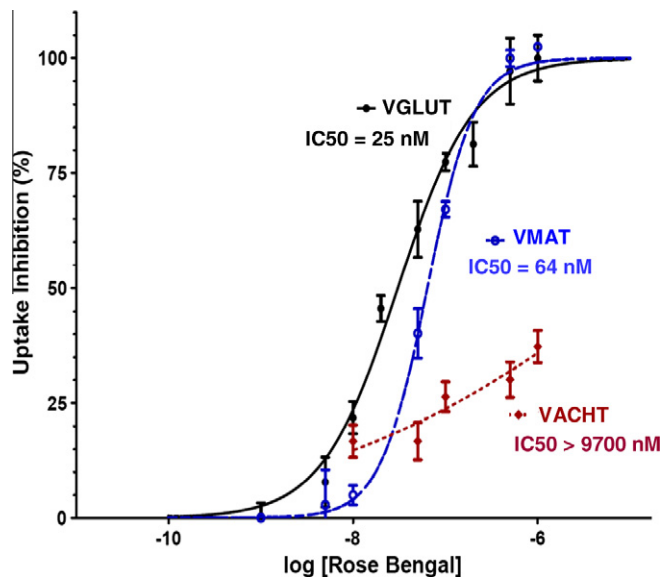

Figure 4. Inhibition of vesicular neurotransmitter uptake: glutamate, 5-HT and acetylcholine by Rose Bengal. These experiments were performed with crude synaptic vesicles from rat brains. Assays could not be run at RB (**2b**) concentrations above 10^{-6} M because of solubility limitation.

VMAT inhibition, RB may be a useful tool to study the mechanism differences between VMAT and VACHT.[72]

Finally, our observations led us to question about the binding site of RB and its analogs. While Ueda has partially addressed that issue and eliminated Na^+/K^+ channel as well as V-ATPase involvement,[36] no unambiguous answer has been provided. Indeed, the neurotransmitter uptake was performed in an entire synaptic vesicle. As Rose Bengal (**2b**) has been described as a non-competitive inhibitor, we could reasonably envisage the possibility for Rose Bengal (**2b**) to indirectly block glutamate uptake by interfering with another protein located upstream of VGLUT in the uptake pathway. For that purpose we have analyzed more carefully reported biological activities of fluorescein derivatives. A brief overview revealed that Erythrosin B (**2a**) was known to inhibit several neurotransmitter uptake[58,73] but also choline acetyltransferase by competitive binding at the adenosine binding site.[74] Interestingly, several publications have reported on the competitive[75–79] and non-competitive kinase inhibition[80] and non-specific enzymatic inhibition[81] of RB (**2b**) but in all these studies, RB acted at higher concentrations than at VGLUTs (micromolar concentrations compared to 25 nM). Since RB is a non-competitive inhibitor of VGLUTs with respect to glutamate and exhibits almost no inhibition of ATP hydrolysis in the uptake assay,[36] it is likely to bind to a specific allosteric site of the transporter. Such ligands are considered to be advantageous as they usually afford higher selectivity than those binding at endogenous substrate (e.g., glutamate or ATP) site. In addition, it was also observed that kinase inhibitors may simultaneously bind at several sites that may be of high and low affinity.[76,82] This situation may also occur presently. Furthermore, Schoichet and collaborators suggested that this non-specific effect could be due to the formation of aggregates that are well known with this kind of dyes.[81] We suggest that RB could act as well as an ATP- or ADP/AMP- competitive binding site inhibitor (but not at the V-ATPase binding site) as it has been observed for some other fluorescein analogs.[75–79]

Indeed, numerous studies have been performed to elucidate the structure–activity requirement for efficient ATP competitive inhibition,[83] and have shown, among other characteristics, the involvement of a flat hydrophobic feature into the ATP binding pocket. Such a feature is actually found in the fluorescein scaffold and in

our pharmacophore model.[84–87] However pharmacophore models of kinase inhibitors are also characterized by at least one hydrogen bond donor or acceptor not present in our model, therefore supporting the hypothesis of an allosteric binding site. We could also envisage a possible interaction of RB with other proteins that take part in the transport of neurotransmitters and are present in the system such as chloride, potassium channels or kinase such as pyruvate kinase[88] or phosphodiesterase.[89] Altogether our data are consistent with a similar high nM affinity binding site of RB at VGLUTs and VMAT2 that is distinct from the weaker affinity and non-specific microM sites that have been described for numerous proteins. With VACHT, RB would only bind to such a weak affinity site.

3. Conclusions

Although the RB analog synthesis may appear to be relatively straightforward in view of the few synthetic steps required, their poor solubility and characterization difficulty encountered during the preparation, made it not so trivial. The structure–activity analysis revealed that the chemical optimization of RB (**2b**) may not be an easy task since halogen substitution remains optimal and introducing any other groups on the xanthyl or phenyl moiety decreased the inhibitory potency. Nevertheless, position 3 of the phenyl ring appeared to be less stringent indicating that the SAR could be extended with a new series of RB esters. These observations were confirmed by the modeling study identifying only hydrophobic features as seems to be required for a good VGLUT inhibition. Our pharmacological studies on VGLUTs, VMAT2 and VACHT, revealed the lack of selectivity of RB (**2b**) between VGLUTs and VMAT2. Yet, our results point out the presence of a high affinity binding site on these two transporters that would deserve future investigations. This site may be an allosteric VGLUT site or situated on another protein required in the vesicular uptake system. Altogether, these results confirm the interest of Rose Bengal and analogs both as potent inhibitors of vesicular glutamate uptake and as potential useful tools for neurotransmitter uptake studies. In particular, if we consider investigation of mechanisms in which both VGLUTs (or VMAT2) and VACHT are involved together.[72] Moreover, we also open the way for selectivity optimization and provide some insights to elucidate the inhibition binding mode of this scaffold.

4. Experimental section

4.1. General

All chemicals and solvents were purchased from commercial suppliers (Acros, Aldrich) and used as received. ^{1}H (250.13 or 500.16 MHz) and ^{13}C (62.9 or 125.78 MHz) NMR spectra were recorded on an ARX 250 or an Avance II 500 Bruker spectrometers. Chemical shifts (δ, ppm) are given with reference to residual ^{1}H or ^{13}C of deuterated solvents (CDCl$_3$ 7.24, 77.00; CD$_3$OD 3.30, 49.0; D$_2$O 4.80). Product visualization was achieved by thin-layer chromatography and was performed on Merck Silica Gel 60 plates with fluorescent indicator. The plates were visualized with UV light (254 nm) or with a 3.5% solution of phosphomolybdic acid in ethanol or with 2% (w/v) ninhydrin in ethanol. Column chromatography was performed with Biotage FLASH40i chromatography module (prepacked cartridge system). Elemental analyses were performed at the ICSN CNRS, Gif-sur-Yvette, France. Melting points were determined in capillary tubes on a Büchi apparatus and are uncorrected. IR spectra of samples were obtained neat with a FT-IR spectrophotometer. Mass spectra (MS) were recorded with a LCQ-advantage (Thermo-Finnigan) mass spectrometer with positive (ESI+) or negative (ESI−)

electrospray ionization (ionization tension 4.5 kV, injection temperature 240 °C). HPLC analyses were carried out on a Gilson analytical instrument with a 321 pump, CC 125/4.0 Nucleosil 100-5 C18 column (Macherey-Nagel, 125 mm × 4 mm), temperature was controlled with an Igloo-CIL Peltier effect thermostat, eluted peaks were detected at 210 nm and 277 nm by a UV–vis 156 detector and retention times are reported in minutes. Products were eluted with a water/methanol mobile phase at 40 °C, a 0.5 mL/min flow rate and detected by UV. The following gradient conditions were used with solvent A (H$_2$O) and solvent B (methanol): 80% A and 20% of B for 3 min, linear increase from 20% to 80% B between 3 and 15 min, 20% A–80% B from 15 min to 25 min. Purity of the tested compounds was established by analytical HPLC and HPLC–MS and was at least 95%.

### 4.2. General methods for the formation of fluorescein derivatives

4.2.1. Method A

Phthalic anhydride or tetrachlorophthalic anhydride (1 equiv) was added to a solution of resorcinol (2 equiv) in methane sulfonic acid (1 M). The resulting mixture was heated under nitrogen at 80–85 °C for 36–48 h. The cooled mixture was poured into six volumes of ice water followed by filtration. The filtrate containing fluorescein or derivatives was dried in vacuo to constant weight.

4.2.2. Method B

Resorcinol (2 equiv) was ground together with phthalic anhydride (1 equiv) and ZnCl$_2$ (0.3 equiv) with a pestle and mortar, and the resulting mixture was heated in a 190 °C oil bath for 30 min. Methanol (about 5 mL/mmol) was added before the medium was cooled down to rt, and the suspension was sonicated for maximum solubilization. Water was then added (about 15 mL/mmol). When a precipitate formed (depending on MeOH and water volumes added, and nature of aromatic substituents), it contained the fluorescein derivative and was filtered. Otherwise the mixture was extracted with DCM. The combined organic layers were washed with brine, dried over MgSO$_4$, and evaporated to afford a yellow to dark orange-brown solid residue. In both methods fluorescein derivatives were obtained in their carboxylic form.

For clarity, atom numbering of lactonic forms has been used.
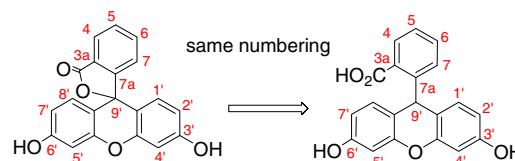
4.2.2.1. 7a-(6′-Hydroxy-3′-oxo-3H-xanthen-9′-yl)benzoic acid (1a).
Method B: 78% yield, yellow solid, mp 320 °C. ^{1}H NMR (DMSO-d_6) δ: 10.11 (s, 2H, OH), 8.02 (d, J = 7.3 Hz, 1H, H4), 7.83–7.70 (m, 2H, H4′, H5′, H6), 7.27 (d, J = 7.3 Hz, 1H, H7), 6.69 (br s, 2H, H1′, H8′), 6.56 (m, 4H, H4′, H5′, H2′, H7′). ^{1}H NMR (MeOD-d4) δ: 8.20 (d, J = 7.3 Hz, 1H, H4), 7.98–7.85 (m, 2H, H5, H6), 7.40 (d, J = 7.3 Hz, 1H, H7), 6.87 (d, J = 2.3 Hz, 2H, H1′, H8′), 6.82 (d, J = 8.7 Hz, 2H, H2′, H7′), 6.73 (dd, 2H, H4′, H5′). ^{13}C (MeOD-d4) δ: 171.5 (Cq), 161.2 (Cq), 161.1 (Cq), 154.0 (Cq), 136.4, 131.0, 130.1, 128.2 (Cq), 125.7, 125.3, 113.4, 111.3 (Cq), 103.5. IR 1597 cm^{-1}. MS (ESI): m/z 331.1 [M−H]$^−$.

4.2.2.2. 4,5,6,7-Tetrachloro-7a-(6′-hydroxy-3′-oxo-3H-xanthen-9′-yl)benzoic acid (1b).
Method A: 76% yield, brown solid, mp >360 °C. ^{1}H NMR (DMSO-d_6) δ: 10.22 (s, 2H, OH), 6.94 (d, J = 8.5 Hz, 2H, H1′, H8′), 6.73 (d, J = 1.9 Hz, 2H, H4′, H5′), 6.57 (dd,

2H, H2′, H7′). ^{13}C NMR (DMSO-d_6) δ: 163.5, 159.9, 152.0, 148.3, 138.8, 134.9, 134.7, 130.3, 128.9, 127.2, 124.1, 112.6, 106.5, 102.3, 81.7. MS (ESI): m/z 425.3 [M−CO$_2$H]$^-$.

4.2.2.3. 4,7-Dichloro-7a-(6′-hydroxy-3′-oxo-3H-xanthen-9′-yl)benzoic acid (1c). Method B: 67% yield, yellow solid, mp >360 °C. ^{1}H NMR (DMSO-d_6) δ: 10.60 (s, 2H, OH), 7.82 (br s, 1H, H5 or H6), 7.73 (br s, 1H, H5 or H6), 6.79 (d, J = 1.9 Hz, 2H, H1′, H8′), 6.69 (br s, 2H, H4′, H5′), 6.58 (m, 2H, H2′, H7′). MS (ESI): m/z 401.3 [M+H]$^+$; MS (ESI): m/z 398.9 [M−H]$^-$.

4.2.2.4. 5,6-Dichloro-7a-(6′-hydroxy-3′-oxo-3H-xanthen-9′-yl)benzoic acid (1d). Method B: 89% yield, yellow solid, mp >360 °C. ^{1}H NMR (DMSO-d_6) δ: 10.18 (s, 2H, OH), 8.29 (s, 1H, H4 or H7), 7.76 (s, 1H, H4 or H7), 6.74–6.69 (m, 4H, H4′, H5′, H1′, H8′), 6.58 (dd, J = 8.5 Hz, J = 2.3 Hz, 2H, H2′, H7′). MS (ESI): m/z 401.3 [M+H]$^+$.

4.2.2.5. 4,5,6,7-Tetrafluoro-7a-(6′-hydroxy-3′-oxo-3H-xanthen-9′-yl)benzoic acid (1e). Method B: 69% yield, brown solid. ^{1}H NMR (DMSO-d_6) δ: 10.28 (s, 2H, OH), 7.03 (d, J = 8.1 Hz, 2H, H1′, H8′), 6.73 (br s, 2H, H4′, H5′), 6.63 (d, J = 8.1 Hz, 2H, H2′, H7′). MS (ESI): m/z 405.3 [M+H]$^+$.

4.2.2.6. 4,5,6,7-Tetrabromo-7a-(6′-hydroxy-3′-oxo-3H-xanthen-9′-yl)benzoic acid (1f). Method B: 60% yield, brown solid. ^{1}H NMR (DMSO-d_6) δ: 10.25 (s, 2H, OH), 6.87 (d, J = 8.7 Hz, 2H, H1′, H8′), 6.67 (br s, 2H, H4′, H5′), 6.56 (d, J = 8.7 Hz, 2H, H2′, H7′). MS (ESI): m/z 646.8 [M−H]$^-$.

4.2.2.7. 7a-(6′-Hydroxy-4′,5′-dimethyl-3′-oxo-3H-xanthen-9′-yl)benzoic acid (1g). Method B: 76% yield, orange powder. ^{1}H NMR (DMSO-d_6) δ: 9.94 (s, 2H, OH), 7.99 (d, J = 7.3 Hz, 1H, H4), 7.83–7.69 (m, 2H, H5, H6), 7.28 (d, J = 7.3 Hz, 1H, H1), 6.62 (d, 2H, J = 8.9 Hz, H1′, H8′), 6.38 (d, 2H, H2′, H7′), 2.30 (s, 6H, CH$_3$). MS (ESI): m/z 359.2 [M−H]$^-$.

4.2.2.8. 7a-(6′-Hydroxy-3′-oxo-3H-xanthen-9′-yl)-7-nitrobenzoic acid and 2-(6′-hydroxy-3′-oxo-3H-xanthen-9′-yl)-4-nitrobenzoic acid (1h). Method B: 63% yield, yellow powder. ^{1}H NMR (MeOD-d4) δ: 8.08 (d, J = 7.8 Hz, 1H, H4), 7.93 (t, J = 7.8 Hz, 1H, H5), 7.50 (d, J = 7.8 Hz, 1H, H6), 6.70 (d, J = 2.3 Hz, 2H, H1′, H8′), 6.38 (d, J = 8.4 Hz, 2H, H4′, H5′), 6.58 (dd, 2H, H2′, H7′). MS (ESI): m/z 376.2 [M−H]$^-$.

4.2.2.9. 7a-(6′-Hydroxy-3′-oxo-3H-xanthen-9′-yl)terephthalic acid and 2-(6′-hydroxy-3′-oxo-3H-xanthen-9′-yl)isophthalic acid (1i). Method B: 51% yield, orange powder, mixture of two isomers, mp >360 °C. ^{1}H NMR (DMSO-d_6) δ: 13.55 (br s, 2H, COOH), 10.27 (s, 4H, OH), 8.41–7.39 (m, 6H, H4, H5, H6, H7), 6.75 (br s, 4H, H1′, H8′), 6.64–6.55 (m, 8H, H4′, H5′, H2′, H7′). MS (ESI): m/z 375.1 [M−H]$^-$.

4.2.2.10. 4-Hydroxy-7a-(6′-hydroxy-3′-oxo-3H-xanthen-9′-yl)benzoic acid (1j). Method B: 39% yield, dark yellow powder. ^{1}H NMR (DMSO-d_6) δ: 10.93 (s, 1H, OH), 10.05 (s, 2H, OH), 7.53 (t, J = 7.8 Hz, 1H, H6), 7.00 (d, J = 7.8 Hz, 1H, H7), 6.65–6.52 (m, 7H, H5, H4′, H5′, H2′, H7′, H1′, H8′). MS (ESI): m/z 347.0 [M−H]$^-$; ESI$^+$: 349.2 [M+H]$^+$.

4.2.2.11. 7a-(6′-Hydroxy-3′-oxo-3H-xanthen-9′-yl)-5-methylbenzoic acid and 2-(6′-hydroxy-3′-oxo-3H-xanthen-9′-yl)-6-methylbenzoic acid (1k). Method B: 87% yield, orange-red powder. ^{1}H NMR (DMSO-d_6) δ: 10.13 (s, 2H, OH), 7.87 (d, 1H, H7 or H4), 7.73–7.53 (m, 1H, H5), 7.14 (d, 1H, H7 or H4), 6.74 (br s, 2H, H1′, H8′), 6.67–6.62 (m, 4H, H4′, H5′, H2′, H7′), 2.42 (s, 3H, CH$_3$). MS (ESI): m/z 345.1 [M−H]$^-$; ESI$^+$: 347.3 [M+H]$^+$.

4.2.2.12. 5-tert-Butyl-7a-(6′-hydroxy-3′-oxo-3H-xanthen-9′-yl)benzoic acid and 6-tert-butyl-2-(6′-hydroxy-3′-oxo-3H-xanthen-9′-yl)benzoic acid (1l). Method B: quantitative yield, yellow pow-

der. ^{1}H NMR (DMSO-d_6) δ: 10.12 (s, 2H, OH), 7.94–7.60 (m, 3H, H7, H5, H4), 6.69 (br s, 2H, H1′, H8′), 6.60–6.52 (m, 4H, H4′, H5′, H2′, H7′), 1.40, 1.33, 1.25 (3s, 9H, tBu). MS (ESI): m/z 387.1 [M−H]$^-$; ESI$^+$: 389.3 [M+H]$^+$.

4.2.2.13. 4,5,6,7-Tetrachloro-7a-(9′-hydroxy-5′-oxo-5H-benzo[a]xanthen-12′-yl)benzoic acid (6). Method B: 27% yield, brown powder. ^{1}H NMR (DMSO-d_6) δ: 11.79 (s, 2H, OH), 8.01–7.52 (m, 4H, H9′, H10′, H11′, H12′), 6.75 (br s, 1H, H1′), 6.60–6.38 (m, 3H, H2′, H4′, H5′). HPLC t_R 15.37 min .MS (ESI): m/z 518.8 [M−H]$^-$.

4.2.2.14. 4,5,6,7-Tetrachloro-7a-(9′-hydroxy-5′-oxo-5H-dibenzo[a,j]xanthen-14′-yl)benzoic acid (7). Method B: 63% yield, brown powder. ^{1}H NMR (DMSO-d_6) δ: 12.07 (s, 2H, OH), 8.01–7.32 (m, 8H, H9′, H10′, H11′, H12′, H13′, H14′, H15′, H16′), 6.65–6.38 (m, 2H, H4′, H5′). HPLC t_R 15.28 min MS (ESI): m/z 569.2 [M−H]$^-$.

4.3. General method for the iodination of fluorescein derivatives

4.3.1. Method C

Iodic acid (2 equiv) was dissolved in a minimum of water and added dropwise to a solution of compound **1** (1 equiv) and iodine (2.5 equiv) in absolute ethanol. This mixture was stirred over 2 h during which the dark brown solution slowly turned red orange. The mixture was then heated to 60 °C for an hour. After cooling, the mixture was filtered and the red solid washed with water and ethanol.

4.3.1.1. 7a-(6′-Hydroxy-2′,4′,5′,7′-tetraiodo-3′-oxo-3H-xanthen-9′-yl)benzoic acid (2a). Method C: 59% yield, red powder, mp 290–292 °C. ^{1}H NMR (DMSO-d_6) δ: 10.24 (br s, 2H, OH), 8.18 (d, J = 7.3 Hz, 1H, H4), 7.86–7.78 (m, 2H, H5, H6), 7.46 (d, J = 7.3 Hz, 1H, H7), 7.27 (s, 1H, H1′ or H8′), 7.02 (s, 1H, H1′ or H8′). HPLC t_R 13.35 min. MS (ESI): m/z 834.7 [M−H]$^-$; MS (ESI): m/z 836.8 [M−H]$^+$.

4.3.1.2. 4,5,6,7-Tetrachloro-7a-(6′-hydroxy-2′,4′,5′,7′-tetraiodo-3′-oxo-3H-xanthen-9′-yl)benzoic acid (2b). Method C: 43% yield, red powder, mp 297–300 °C. ^{1}H NMR (MeOD-d4) δ: 7.59 (s, 2H, H1′, H8′). HPLC t_R 15.80 min. MS (ESI): m/z 972.4 [M−H]$^-$; MS (ESI): m/z 974.6 [M−H]$^+$.

4.3.1.3. 4,7-Dichloro-7a-(6′-hydroxy-2′,4′,5′,7′-tetraiodo-3′-oxo-3H-xanthen-9′-yl)benzoic acid (2c). Method C: 49% yield, red powder, mp >320 °C. ^{1}H NMR (DMSO-d_6) δ: 10.25 (s, 2H, OH), 7.86 (br s, 2H), 7.43 (br s, 2H). HPLC t_R 13.97 min. MS (ESI): m/z 902.5 [M−H]$^-$; MS (ESI): m/z 904.7 [M−H]$^+$.

4.3.1.4. 5,6-Dichloro-7a-(6′-hydroxy-2′,4′,5′,7′-tetraiodo-3′-oxo-3H-xanthen-9′-yl)benzoic acid (2d). Method C: 48% yield, red powder, mp >320 °C. ^{1}H NMR (CDCl$_3$) δ: 8.16 (s, 1H, H4), 7.25 (s, 2H, H1′, H8′), 7.14 (s, 1H, H7). HPLC t_R 14.80 min. MS (ESI): m/z 902.6 [M−H]$^-$; MS (ESI): m/z 904.7 [M−H]$^+$.

4.3.1.5. 4,5,6,7-Tetrafluoro-7a-(6′-hydroxy-2′,4′,5′,7′-tetraiodo-3′-oxo-3H-xanthen-9′-yl)benzoic acid (2e). Method C: 56% yield, red powder, mp 294 °C. ^{1}H NMR (DMSO-d_6) δ: 10.33 (s, 2H, OH), 7.66 (s, 2H, H1′, H8′). HPLC t_R 12.07 min. MS (ESI): m/z 906.7 [M−H]$^-$; ESI$^+$: 908.6 [M−H]$^+$.

4.3.1.6. 4,5,6,7-Tetrabromo-7a-(6′-hydroxy-2′,4′,5′,7′-tetraiodo-3′-oxo-3H-xanthen-9′-yl)benzoic acid (2f). Method C: 37% yield, red powder, mp 284–286 °C. ^{1}H NMR (DMSO-d_6) δ: 10.22 (s, 2H, OH), 7.51 (s, 2H, H1′, H8′). HPLC t_R 14.53 min. MS (ESI): m/z 1150.2 [M−H]$^-$.

4.3.1.7. 7a-(6′-Hydroxy-2′,7′-diiodo-4′,5′-dimethyl-3′-oxo-3*H*-xanthen-9′-yl)benzoic acid (2g). Method C: 37% yield, red powder, decomp., mp 190 °C. HPLC t_R 17.87 min. MS (ESI): *m/z* 610.7 [M−H]⁻.

4.3.1.8. 7a-(6′-Hydroxy-2′,4′,5′,7′-tetraiodo-3′-oxo-3*H*-xanthen-9′-yl)-4-nitrobenzoic acid and 7a-(6′-hydroxy-2′,4′,5′,7′-tetraiodo-3′-oxo-3*H*-xanthen-9′-yl)-7-nitrobenzoic acid (2h). Method C: 45% yield, red powder, mp >320 °C. HPLC t_R 11.82 min. MS (ESI): *m/z* 879.7 [M−H]⁻; MS (ESI): *m/z* 881.7 [M−H]⁺.

4.3.1.9. 7a-(6′-Hydroxy-2′,4′,5′,7′-tetraiodo-3′-oxo-3*H*-xanthen-9′-yl)terephthalic acid and 7a-(6′-hydroxy-2′,4′,5′,7′-tetraiodo-3′-oxo-3*H*-xanthen-9′-yl)isophthalic acid (2i). Method C: 56% yield, red powder, mp >320 °C. HPLC t_R 12.61 min. MS (ESI): *m/z* 878.7 [M−H]⁻; MS (ESI): *m/z* 880.7 [M−H]⁺.

4.3.1.10. 4-Hydroxy-7a-(6′-hydroxy-2′,4′,5′,7′-tetraiodo-3′-oxo-3*H*-xanthen-9′-yl)benzoic acid (2j). Method C: 21% yield, red powder, mp >320 °C. HPLC t_R 12.42 min. MS (ESI): *m/z* 850.6 [M−H]⁻.

4.3.1.11. 7a-(6′-Hydroxy-2′,4′,5′,7′-tetraiodo-3′-oxo-3*H*-xanthen-9′-yl)-5-methylbenzoic acid and 7a-(6′-hydroxy-2′,4′,5′,7′-tetraiodo-3′-oxo-3*H*-xanthen-9′-yl)-6-methylbenzoic acid (2k). Method C: 43% yield, red powder, mp >320 °C. HPLC t_R 13.05 min. MS (ESI): *m/z* 848.7 [M−H]⁻; MS (ESI): *m/z* 850.8 [M−H]⁺.

4.3.1.12. 5-*tert*-Butyl-7a-(6′-hydroxy-2′,4′,5′,7′-tetraiodo-3′-oxo-3*H*-xanthen-9′-yl)benzoic acid and 6-*tert*-butyl-7a-(6′-hydroxy-2′,4′,5′,7′-tetraiodo-3′-oxo-3*H*-xanthen-9′-yl)benzoic acid (2l).
Method C: 39% yield, red powder, mp >320 °C. HPLC t_R 14.62 min. MS (ESI): *m/z* 890.7 [M−H]⁻; MS (ESI): *m/z* 892.8 [M−H]⁺.

4.3.2. Method D. Esterification
4.3.2.1. Ethyl 4,5,6,7-tetrachloro-7a-(6′-hydroxy-2′,4′,5′,7′-tetraiodo-3′-oxo-3*H*-xanthen-9′-yl)benzoate (3). Compound **2b** (0.06 mmol, 1 equiv) was suspended in 10 mL THF. Ethylene bromide solution (1 equiv in 250 μL of THF) was then added as well as a DBU solution (1 equiv in 50 μL). The solution was heated at 65 °C overnight. The mixture was extracted with DCM/H₂O, the organic layer was dried and purified by extraction with aq. HCl/DCM. A red powder was obtained in a low yield (15.6 mg, 26.5%). HPLC t_R 18.12 min. MS (ESI): *m/z* 1000.6 [M−H]⁻.

4.3.2.2. Ethyl 2-(2′,7′-dibromo-6′-hydroxy-4′-5′-dinitro-3′-oxo-3*H*-xanthen-9′-yl)benzoate (8). Eosin B (**BU8**, 580 mg, 1 mmol) and potassium hydroxide (200 mg, 3.5 mmol) were dissolved in distilled THF (10 mL). The reaction mixture was stirred under argon for 30 min. Then ethyl bromide (272.4 mg, 2.5 mmol) and DBU (372 μL, 2.5 mmol) were added and the reaction was heated under argon at 70 °C for 72 h. After cooling down to room temperature, the reaction mixture was extracted with ethyl acetate (2 × 100 mL). The organic layer was washed with two portions of brine and dried over anhydrous MgSO₄. The solvent was evaporated at reduced pressure. The red crude product was purified by PLC (Silica Gel 60 F₂₅₄, 2 mm). Elution with DCM/MeOH (90/10) afforded **8** as a red-violet powder (0.284 g, yield 46.7%). HPLC t_R 3.27 min. MS (ESI): *m/z* 606.9 [M−H]⁻. Mp >320 °C.

4.3.3. Method E. Etherification
4.3.3.1. 4,5,6,7-Tetrachloro-7a-(2′,4′,5′,7′-tetraiodo-6′-methoxy-3′-oxo-3*H*-xanthen-9′-yl)benzoic acid (4). Rose Bengal lactone (0.13 mmol, 1 equiv) was suspended in 5 mL DMF with potassium

carbonate (2.2 equiv) at 0 °C. Methyl iodide (2.2 equiv) was then added dropwise, the mixture was warmed to room temperature and stirred for 17 h. Residual methyl iodide was quenched by a mixture of ice/water and extracted with AcOEt/H₂O. The organic layer was dried over MgSO₄, filtered and evaporated to give a violet solid (31.3 mg, 24% yield). HPLC t_R 10.35 min. MS (ESI): *m/z* 986.5 [M−H]⁻.

4.3.3.2. 4,5,6,7-Tetrachloro-2′,4′,5′,7′-tetraiodo-3′,6′-dimethoxy-3*H*-spiro[isobenzofuran-1,9′-xanthen]-3-one (5). Compound **4** (0.13 mmol, 1 equiv) was suspended in 5 mL DMF with potassium carbonate (2.2 equiv) at 0 °C. Methyl iodide (2.2 equiv) was then added dropwise; the mixture was warmed to room temperature and stirred for 17 h. K₂CO₃ (5 equiv) was then added and the mixture was stirred for two more days. Residual methyl iodide was quenched by a mixture of ice/water and extracted with AcOEt/H₂O. The organic layer was dried and evaporated to afford a violet solid (13.5 mg, 42.6% yield). HPLC t_R 7.36 min. MS (ESI): *m/z* 1000.6 [M+H]⁺.

4.4. Subcellular fractionation and amino acid uptake assay

Rats or mice were killed by decapitation. Brains were removed and the striatum, cerebral cortex, hippocampus and brainstem were dissected on ice and resuspended in ice-cold sucrose (0.32 M). Striatal synaptic vesicles were purified as described.[90] Synaptic vesicle pellets from 30 rat brains or 61 mouse brains were resuspended in ice-cold 0.32 M sucrose, 4 mM KCl, 4 mM MgSO4 and 10 mM HEPES–KOH, pH 7.4 (uptake buffer).

4.5. Vesicular neurotransmitter transport assay

The Vesicular Glutamate uptake was assayed by a modification of the method of Naito and Ueda[25] as described by Kish and Ueda.[91] Aliquots (10 μg) of crude rat synaptic vesicles were incubated for 10 min at 30 °C in a solution containing 20 mM HEPES–KOH, pH 7.4, 0.25 mM sucrose, 4 mM MgSO₄, 4 mM KCl, 2 mM L-aspartic acid, 50 μM Glu, 2 mM ATP, and 2 mCi (40 mM) [³H]Glu (Amersham) in a final volume of 0.1 mL. Test compounds were dissolved in DMSO and added in 0.6 μL aliquots to give final concentrations between 0.14 nM and 25 μM. Synaptic vesicles were preincubated with test compounds for 30 min at 0 °C. Uptake was initiated by addition of a mixture A of 2 mM ATP and 50 μM Glu (final concentration) containing 1 μCi of [³H]Glu. After 10 min at 30 °C, 2.5 mL of ice-cold 0.15 m KCl were added and the mixture immediately filtered through Whatman GF/C glass–fiber filter paper (25 mm) using a manifold under vacuum. The filters were washed five times with 2.5 mL of 0.15 M KCl and placed in scintillation vials with scintillation cocktail (Cytoscint, ICN). The vials were shaken overnight and radioactivity determined in a Beckman LS 6500 scintillation spectrophotometer. Values obtained in the absence of ATP were subtracted from those in the presence of ATP to calculate ATP dependent uptake activity. The amount of radioactive Glu trapped on GF/C glass–fiber filter paper was indistinguishable from that trapped on the Millipore HAWP filter (data not shown). Since the rate of filtration with GF/C glass-fiber filter paper is greater, this type of filter was used in all experiments described here.

The glutamate uptake was also performed on 96-well plate (Millipore MultiScreen_HTS-HA Plate) using MultiScreen-HTS Vacuum Manifold as filtration support, all the previous concentrations were conserved and we processed as follow: first, a pre-incubation of synaptic vesicles with/without inhibitors in a total of 50 μL of buffer was performed; next, uptake was initiated by addition of solution A containing ATP and 1 μCi of [³H]Glu. The uptake was stopped by addition of 0.15 M of ice-cold KCl (each well was

washed five times). The same controls were used for the evaluation of inhibitory efficiency.

Other neurotransmitter uptake was performed with similar protocols. Briefly, Rat synaptic vesicles are incubated with appropriated neurotransmitter, buffer and inhibitor. The uptake is then stopped by addition of cold potassium chloride.[62] The residual radioactivity is measured and the inhibition is calculated from 0% given by uptake without inhibitor and 100% given by the radioactivity measure in absence of ATP.

4.6. VGLUT pharmacophore model generation

Molecule sketching, conformation generation, feature edition and pharmacophore model generation were performed using Discovery Studio version 2.5 (Accelrys Inc., San Diego CA) which launched the suitable Catalyst standalone executables via a PipelinePilot server.

4.6.1. Statistical significance

To evaluate if the SAR content of the training set was indeed reflected by the selected model, a Fischer test was performed by shuffling the measured activity values of the training set 49 times (Catalyst-CatScramble) and running Catalyst-Hypogen with these artificial datasets. Since none of the models generated with the 49 artificial datasets could perform better than the original set, it was concluded that the significance of the model obtained with our training set was at least of 98%.

4.6.2. ROC curve analysis

A ROC curve analysis[92] was performed in order to evaluate the ability of the model to correctly discriminate the most active molecules (below 900nM) from the least active ones (above 900nM). The selected model exhibited areas under the curve (AUCs) of 0.94 and 0.86 when the training set and the whole dataset were, respectively, considered. Last a Fisher test was performed on the overall dataset to assess the likelihood that the ROC performance of the retained model was due to shear chance. Hence, by shuffling 99 times the measured activities within the whole dataset one can calculate 99 ROC AUCs. Since none of the determined AUC was higher than 0.86, the Fischer statistical test allowed to assert that the significance of the model is at least 99%.

Acknowledgments

Supplementary data

Supplementary data associated with this article can be found, in the online version, at doi:10.1016/j.bmc.2010.06.069.

References and notes

1. Thompson, C. M.; Davis, E.; Carrigan, C. N.; Cox, H. D.; Bridges, R. J.; Gerdes, J. M. *Curr. Med. Chem.* **2005**, *12*, 2041.
2. Shigeri, Y.; Seal, R. P.; Shimamoto, K. *Brain Res. Rev.* **2004**, *45*, 250.
3. Nicholls, D. G. *J. Neurochem.* **1989**, *52*, 331.
4. Maycox, P. R.; Deckwerth, T.; Jahn, R. *EMBO J.* **1990**, *9*, 1465.
5. Ozkan, E. D.; Ueda, T. *Jpn. J. Pharmacol.* **1998**, *77*, 1.
6. Stormmathisen, J.; Leknes, A. K.; Bore, A. T.; Vaaland, J. L.; Edminson, P.; Haug, F. M. S.; Ottersen, O. P. *Nature* **1983**, *301*, 517.
7. Burger, P. M.; Mehl, E.; Cameron, P. L.; Maycox, P. R.; Baumert, M.; Lottspeich, F.; Decamilli, P.; Jahn, R. *Neuron* **1989**, *3*, 715.
8. Meldrum, B. *Clin. Sci.* **1985**, *68*, 113.
9. Choi, D. W. *Neuron* **1988**, *1*, 623.
10. Javitt, D. C.; Zukin, S. R. *Am. J. Psychiatry* **1991**, *148*, 1301.
11. Zorumski, C. F.; Olney, J. W. *Pharmacol. Ther.* **1993**, *59*, 145.
12. Lipton, S. A.; Rosenberg, P. A. *N. Eng. J. Med.* **1994**, *330*, 613.
13. Bradford, H. F. *Prog. Neurobiol.* **1995**, *47*, 477.
14. Olney, J. W.; Farber, N. B. *Arch. Gen. Psychiat.* **1995**, *52*, 998.
15. Coyle, J. T. *Harvard Rev. Psychiatry* **1996**, *3*, 241.
16. Chapman, A. G. *Prog. Brain Res.* **1998**, *116*, 371.
17. Lepicard, E.; Poirel, O.; Kashani, A.; Amilhon, B.; Hirsch, E.; Epelbaum, J.; David, J. P.; Delacourte, J.; Giros, B.; Betancur, C.; El Mestikawy, S. *Eur. Neuropsychopharmacol.* **2007**, *17*, S534.
18. Bellocchio, E. E.; Reimer, R. J.; Fremeau, R. T.; Edwards, R. H. *Science* **2000**, *289*, 957.
19. Bai, L. Q.; Xu, H.; Collins, J. F.; Ghishan, F. K. *J. Biol. Chem.* **2001**, *276*, 36764.
20. Herzog, E.; Bellenchi, G. C.; Gras, C.; Bernard, V.; Ravassard, P.; Bedet, C.; Gasnier, B.; Giros, B.; El Mestikawy, S. *J. Neurosci.* **2001**, *21*, 22.
21. Gras, C.; Herzog, E.; Bellenchi, G. C.; Bernard, V.; Ravassard, P.; Pohl, M.; Gasnier, B.; Giros, B.; El Mestikawy, S. *J. Neurosci.* **2002**, *22*, 5442.
22. Kashani, A.; Lepicard, E.; Poirel, O.; Videau, C.; David, J. P.; Fallet-Bianco, C.; Simon, A.; Delacourte, A.; Giros, B.; Epelbaum, J.; Betancur, C.; El Mestikawy, S. *Neurobiol. Aging* **2008**, *29*, 1619.
23. Takamori, S. *Neurosci. Res.* **2006**, *55*, 343.
24. Francis, P. T. *Int. J. Geriatr. Psychiatry* **2003**, *18*, S15.
25. Naito, S.; Ueda, T. *J. Neurochem.* **1985**, *44*, 99.
26. Winter, H. C.; Ueda, T. *Neurochem. Res.* **1993**, *18*, 79.
27. Carlson, M. D.; Kish, P. E.; Ueda, T. *J. Neurochem.* **1989**, *53*, 1889.
28. Moriyama, Y.; Amakatsu, K.; Yamada, H.; Park, M. Y.; Futai, M. *Arch. Biochem. Biophys.* **1991**, *290*, 233.
29. Carrigan, C. N.; Esslinger, C. S.; Bartlett, R. D.; Bridges, R. J.; Thompson, C. M. *Bioorg. Med. Chem. Lett.* **1999**, *9*, 2607.
30. Roseth, S.; Fykse, E. M.; Fonnum, F. *J. Neurochem.* **1995**, *65*, 96.
31. Roseth, S.; Fykse, E. M.; Fonnum, F. *Biochem. Pharmacol.* **1998**, *56*, 1243.
32. Moriyama, Y.; Yamamoto, A. *J. Biol. Chem.* **1995**, *270*, 22314.
33. Bole, D. G.; Ueda, T. *Neurochem. Res.* **2005**, *30*, 363.
34. Bartlett, R. D.; Esslinger, C. S.; Thompson, C. M.; Bridges, R. J. *Neuropharmacology* **1998**, *37*, 839.
35. Carrigan, C. N.; Bartlett, R. D.; Esslinger, C. S.; Cybulski, K. A.; Tongcharoensirikul, P.; Bridges, R. J.; Thompson, C. M. *J. Med. Chem.* **2002**, *45*, 2260.
36. Ogita, K.; Hirata, K.; Bole, D. G.; Yoshida, S.; Tamura, Y.; Leckenby, A. M.; Ueda, T. *J. Neurochem.* **2001**, *77*, 34.
37. von Bayer, A. *Chem. Ber.* **1871**, *5*, 255.
38. Burdette, S.; Walkup, G.; Spingler, B.; Tsien, R.; Lippard, S. *J. Am. Chem. Soc.* **2001**, *123*, 7831.
39. Sun, W. C.; Gee, K. R.; Klaubert, D. H.; Haugland, R. P. *J. Org. Chem.* **1997**, *62*, 6469.
40. Ueno, Y.; Jiao, G. S.; Burgess, K. *Synthesis (Stuttgart)* **2004**, *15*, 2591.
41. Schmidt, H. W. *Synthesis (Stuttgart)* **1985**, *8*, 778.
42. Hirano, T.; Kikuchi, K.; Urano, Y.; Nagano, T. *J. Am. Chem. Soc.* **2002**, *124*, 6555.
43. Lukhtanov, E. A.; Vorobiev, A. V. *J. Org. Chem.* **2008**, *73*, 2424.
44. Rossi, F. M.; Kao, J. P. Y. *Bioconjugate Chem.* **1997**, *8*, 495.
45. Woodroofe, C. C.; Lim, M. H.; Bu, W. M.; Lippard, S. J. *Tetrahedron* **2005**, *61*, 3097.
46. Lyttle, M. H.; Carter, T. G.; Cook, R. M. *Org. Process Res. Dev.* **2001**, *5*, 45.
47. Coan, K. E. D.; Shoichet, B. K. *J. Am. Chem. Soc.* **2008**, *130*, 9606.
48. Klonis, N.; Sawyer, W. H. *Photochem. Photobiol.* **2000**, *72*, 179.
49. Alvarez-Pez, J. M.; Ballesteros, L.; Talavera, E.; Yguerabide, J. *J. Phys. Chem. A* **2001**, *105*, 6320.
50. Hwang, S. G.; Jang, Y. H.; Chung, D. S. *Chem. Lett.* **2001**, *11*, 1182.
51. Anthoni, U.; Christophersen, C.; Nielsen, P. H.; Puschl, A.; Schaumburg, K. *Struct. Chem.* **1995**, *6*, 161.
52. Lavis, L. D.; Rutkoski, T. J.; Raines, R. T. *Anal. Chem.* **2007**, *79*, 6775.
53. Samoilov, D. V.; Mchedlov-Petrosyan, N. O.; Martynova, V. P.; El'tsov, A. V. *Russ. J. Gen. Chem.* **2000**, *8*, 1259.
54. Mchedlov-Petrossyan, N. O.; Vodolazkaya, N. A.; Surov, Y. N.; Samoylov, D. V. *Spectrochim. Acta A* **2005**, *61*, 2747.
55. Brenzovich, W. E.; Odell, M. D.; Soares, J. P.; Abelt, C. J. *Dyes Pigments* **2003**, *59*, 251.
56. Tamura, Z.; Terada, R.; Ohno, K.; Maeda, M. *Anal. Sci.* **1999**, *15*, 339.
57. Xu, D.; Vanloon, A.; Linden, S. M.; Neckers, D. C. *J. Photochem.* **1987**, *38*, 357.
58. Amatguerri, F.; Lopezgonzalez, M. M. C.; Martinezutrilla, R.; Sastre, R. *Dyes Pigments* **1990**, *12*, 249.
59. Klonis, N.; Clayton, A. H. A.; Voss, E. W.; Sawyer, W. H. *Photochem. Photobiol.* **1998**, *67*, 500.
60. Mchedlov-Petrosyan, N. O.; Rubtsov, M. I.; Lukatskaya, L. L. *Russ. J. Gen. Chem.* **2000**, *8*, 1177.
61. Mchedlov-Petrosyan, N. O.; Vodolazkaya, N. A.; Martynova, V. P.; Samoilov, D. V.; El'tsov, A. V. *Russ. J. Gen. Chem.* **2002**, *5*, 785.
62. Gras, C.; Amilhon, B.; Lepicard, E. M.; Poirel, O.; Vinatier, J.; Herbin, M.; Dumas, S.; Tzavara, E. T.; Wade, M. R.; Nomikos, G. G.; Hanoun, N.; Saurini, F.; Kemel, M. L.; Gasnier, B.; Giros, B.; El Mestikawy, S. *Nat. Neurosci.* **2008**, *11*, 292.
63. Carreon, J. R.; Roberts, M. A.; Wittenhagen, L. M.; Kelley, S. O. *Org. Lett.* **2005**, *7*, 99.

64. Sugita, N.; Kawabata, K.; Sasaki, K.; Sakata, I.; Umemura, S. *Bioconjugate Chem.* **2007**, *18*, 866.
65. Lu, Y. X.; Shi, T.; Wang, Y.; Yang, H. Y.; Yan, X. H.; Luo, X. M.; Jiang, H. L.; Zhu, W. L. *J. Med. Chem.* **2009**, *52*, 2854.
66. Smellie, A.; Kahn, S. D.; Teig, S. L. *J. Chem. Inf. Comput. Sci* **1995**, *35*, 285.
67. Smellie, A.; Teig, S. L.; Towbin, P. *J. Comput. Chem.* **1995**, *16*, 171.
68. Li, H.; Sutter, J.; Hoffmann, R., HypoGen: an automated system for generating 3D predictive pharmacophore models. In *Pharmacophore Perception, Development, and Use in Drug Design*, Guner, O. F. Ed. International University Line: La Jolla, CA: 2000; Vol. 2, pp 171.
69. Chaudhry, F. A.; Edwards, R. H.; Fonnum, F. *Annu. Rev. Pharmacol. Toxicol.* **2008**, *48*, 277.
70. Amilhon, B.; El Mestikawy, S. *M S-Med. Sci.* **2008**, *24*, 1009.
71. Fredriksson, R.; Nordstrom, K. J.; Stephansson, O.; Hagglund, M. G.; Schioth, H. B. *FEBS Lett.* **2008**, *582*, 3811.
72. Parsons, S. M. *FASEB J.* **2000**, *14*, 2423.
73. Logan, W. J.; Swanson, J. M. *Science* **1979**, *206*, 363.
74. Mautner, H. G.; Merrill, R. E.; Currier, S. F.; Harvey, G. *J. Med. Chem.* **1981**, *24*, 1534.
75. Deweille, J. R.; Muller, M.; Lazdunski, M. *J. Biol. Chem.* **1992**, *267*, 4557.
76. Cai, Z. W.; Sheppard, D. N. *J. Biol. Chem.* **2002**, *277*, 19546.
77. Karlish, S. J. D. *J. Bioenerg. Biomembr.* **1980**, *12*, 111.
78. Neslund, G. G.; Miara, J. E.; Kang, J. J.; Dahms, A. S. *Curr. Top Cell. Regul.* **1984**, *24*, 447.
79. Ogan, J. T.; Reifenberger, M. S.; Milanick, M. A.; Gatto, C. *Blood Cell Mol. Dis.* **2007**, *38*, 229.
80. Hopkins, S. C.; Vale, R. D.; Kuntz, I. D. *Biochemistry-Us* **2000**, *39*, 2805.
81. McGovern, S. L.; Caselli, E.; Grigorieff, N.; Shoichet, B. K. *J. Med. Chem.* **2002**, *45*, 1712.
82. Bachmann, A.; Russ, U.; Waldegger, S.; Quast, U. *Br. J. Pharmacol.* **2000**, *131*, 433.
83. McGregor, M. J. *J. Chem. Inf. Model.* **2007**, *47*, 2374.
84. Knight, Z. A.; Shokat, K. M. *Chem. Biol.* **2005**, *12*, 621.
85. Xie, Q. Q.; Xie, H. Z.; Ren, J. X.; Li, L. L.; Yang, S. Y. *J. Mol. Graphics Modell.* **2009**, *27*, 751.
86. Baldwin, I.; Bamborough, P.; Haslam, C. G.; Hunjan, S. S.; Longstaff, T.; Mooney, C. J.; Patel, S.; Quinn, J.; Somers, D. O. *Bioorg. Med. Chem. Lett.* **2008**, *18*, 5285.
87. Noble, M. E. M.; Endicott, J. A.; Johnson, L. N. *Science* **2004**, *303*, 1800.
88. Ishida, A.; Noda, Y.; Ueda, T. *Neurochem. Res.* **2009**, *34*, 807.
89. Reyes-Irisarri, E.; Perez-Torres, S.; Mengod, G. *Neuroscience* **2005**, *132*, 1173.
90. Huttner, W. B.; Schiebler, W.; Greengard, P.; De Camilli, P. *J. Cell Biol.* **1983**, *96*, 1374.
91. Kish, P. E.; Ueda, T. *Method Enzymol.* **1989**, *174*, 9.
92. Triballeau, N.; Acher, F.; Brabet, I.; Pin, J. P.; Bertrand, H. O. *J. Med. Chem.* **2005**, *48*, 2534.